Comparative study of hybrid nanofluids in microchannel slip flow induced by electroosmosis and peristalsis

Beg, OA, Prakash, J and Tripathi, D

http://dx.doi.org/10.1007/s13204-020-01286-1

APPLIED NANOSCIENCE (SPRINGER)

Accepted February 8th 2020

COMPARATIVE STUDY OF HYBRID NANOFLUIDS IN MICROCHANNEL SLIP FLOW INDUCED BY ELECTROOSMOSIS AND PERISTALSIS

[1]Jayavel Prakash, [*2]Dharmendra Tripathi *and* **[3]O. Anwar Bég**

[1]Department of Mathematics, Avvaiyar Government College for Women, Karaikal-609 602, Puducherry –U.T., ***India.***

[2]Department of Mathematics, National Institute of Technology Uttarakhand, Srinagar -246174, ***India***

[3]Professor, Multi-Physical Engineering, Dept. Mechanical Engineering, SEE, Salford University, Manchester, M54WT, ***UK.***

****Corresponding author: dtripathi@nituk.ac.in***

ABSTRACT

In this paper, a mathematical model is developed to investigate the electroosmotic flow of hybrid nanoliquids (containing dissimilar nanoparticles) through an asymmetric microchannel which is moving sinusoidally with constant wave velocity under an axial electrical field. The effects of Joule heating are included. Maxwell and Brinkmann correlations are employed for nanoliquid thermal conductivity and viscosity. To study the performance of hybrid nanofluids, a selection of nanofluids is examined with water as the base fluid which is doped with titania, alumina or copper metallic nanoparticles. The boundary conditions include velocity slip and thermal slip at the microchannel walls. The Debye-Hückel linearization is employed. Numerical computations for velocity, pressure gradient and temperature fields are executed in the MATLAB bvp4c routine. The influence of selected physical parameters on the flow characteristics, pumping characteristics, and temperature distribution are computed. Pressure gradient is elevated with stronger buoyancy i.e. higher thermal Grashof number and also electroosmosis parameter whereas it is suppressed with greater velocity slip and thermal slip parameters. Axial flow is strongly accelerated with increasing Joule heating parameter and velocity slip. Periodic behavior is observed for axial pressure gradient for all three metallic nanoparticles due to the sinusoidal nature of the pumping. With increasing Brinkman number (dissipation parameter), axial pressure gradient is decreased for alumina (Al_2O_3). Temperature is strongly increased with greater Joule heating parameter across the microchannel width for *Cu-water* nanoliquid. Temperature is increased for (Al_2O_3)-water nanofluid in the left microchannel half space with increasing thermal Grashof Number whereas it is decreased in the right half space. Temperatures are enhanced for titania TiO_2 -water nanoliquid in the left half space with greater velocity slip parameter whereas they are diminished in the right half space. The present analysis is relevant to bio-inspired electrokinetic nanofluid micropump designs and emerging nanomedicine technologies.

Keywords: *Electroosmosis; Asymmetric microchannel; Joule heating; thermal and velocity slip conditions; peristaltic pumping; hybrid nanoliquids; metallic nanoparticles; pressure gradient.*

1. INTRODUCTION

Hybrid nanofluids constitute a novel variety of nanoscale fluids in which different size and material metallic nanoparticles are embedded in a base fluid to achieve superior thermal performance and synergy. They are a modification of conventional nanofluids therefore, since

dissimilar nanoparticles are suspended simultaneously in the carrier liquid either in mixture or composite form. Hybrid nanofluids hare increasingly being utilized in various branches of nanotechnology including medicine, smart pumping systems, coatings, fuels, adhesives and lubricants. Many experimental and analytical studies of hybrid nanofluids have been communicated in recent years. These effectively modify the single-phase approach in Choi nanofluids to a mixture model approach for hybrid nanofluids. Suresh *et al.* [1] reported on detailed experiments for fully developed laminar convective heat transfer through a uniformly heated circular tube using Al_2O_3–Cu/water hybrid nanofluid. Sarkar *et al.* [2] presented an interesting review on hybrid nanofluids was presented to analyze recent developments and applications in thermal, medical and industrial engineering systems. Thermophysical properties of hybrid nanofluid (Al_2O_3–Cu/water) have been investigated through experimentation using a two-step synthesis method by Suresh *et al*. [3]. Moghadassi *et al.* [4] conducted a finite volume numerical study on forced convective heat transfer of water-based Al_2O_3–Cu hybrid nanofluids with 0.1% volume concentration and average particle size of 15 nm, observing that the average Nusselt number increases by 4.73% and 13.46% as compared to Al_2O_3/water and pure water, respectively. Minea [5] computed the performance of hybrid nanofluids using Al_2O_3, TiO_2 and SiO_2, noting that all the thermophysical properties and thermal conductivity are increasing by at least 12%. A mathematical model was developed to analyze the heat transfer enhancement of Ag–CuO/water hybrid nanofluid by Hayat and Nadeem [6] using BVP-4C quadrature in MATLAB software. In this direction, many numerical and experimental investigations [7-12] on hybrid nanofluids with various nanoparticles and applications in various emerging fields have been presented in the scientific literature including petro-chemical drilling muds, electronic thermal management, solar collectors and smart coatings. Substantial enhancement in thermophysical properties e.g. thermal conductivity of hybrid nanofluids has been confirmed in these investigations.

Electro-osmosis is an electro-kinetic mechanism in which ions migrate in an electrolyte solution relative to a charged substrate under the influence of an external electric field. This mechanism finds important applications in examining the physical properties and transport phenomena at very small scales (i.e. microscale engineering). It features extensively in diagnostic procedures in health care, designing microchips for small volume transport and the precise mixing of chemicals. Considering the superiority of electro-osmotic designs, instant output and considerable economic benefits, significant interest has been stimulated in modelling electroosmotic flows of nanofluids

and also hybrid nanofluids. Nanofluid electro-osmotic systems combine the efficiency of electro-osmosis with the thermal advantages of nanofluids and offer great potential in 21st century synergistic designs which may also feature other multi-physical phenomena including magneteohydrodynamics (MHD), entropy generation and minimization, ciliated walls, deformable geometry, turbulence, multi-mode heat transfer, non-Newtonian (rheological) characteristics etc. Shehzad *et al.* [13] studied electroosmotic MHD power-law Al_2O_3-PVC nanofluid Couette-Poiseuille flow. Deng [14] studied the fully developed flow driven by electroosmosis of power law nanofluids, noting that heat transfer rates are enhanced for shear-thickening (dilatant) nanofluids and with greater nanoparticle volume fraction. Sheikhizad and Kalteh [15] have computed the heat transfer in periodic electroosmotic flow of nanofluids using the Poisson-Boltzmann method. Zhao and Jian [16] have analyzed the electroosmosis and pressure driven nanofluid flow in soft nanochannels and they have reported that possibility of alteration in the nanofluid heat transfer via nanoparticle volume (percentage doping). However the natural mechanism i.e. peristaltic pumping was ignored in the above investigations.

Peristaltic pumping is a natural pumping process which has been embraced in modern engineering and industrial systems for improving transport mechanisms. Many advanced/smart peristaltic pumps are being designed and commercialized in the market as per the demands of 21st century technology and society. Considering the challenging demands of the peristaltic pumping process, some mathematical models [17-22] have been developed to examine the effects of various parameters on the pumping and flow characteristics which are intrinsic to the optimization of more efficient pumps. These investigations have discussed various applications in the field of biomedical engineering. Nevertheless, none of the studies focused on the combined effects of peristaltic and electroosmotic pumping processes to enhance performance efficiency of smart pumps for fulfilling the need of nanotechnology and health care. By addressing the dual benefits of both pumping mechanisms, several mathematical models [23-27] have been presented to analyze how electroosmosis controls/amplifies the peristaltic pumping process. Prakash and Tripathi [23] have studied radiative heat flux effects in electroosmotic driven peristaltic flow of Williamson viscoelastic ionic nanoliquids through microfluidic channels. Prakash *et al.* [24] examined the electro-osmotic driven peristaltic pumping of pseudoplastic nanofluid in a conduit. Tripathi *et al.* [25] have discussed the Joule heating and buoyancy effects in electro-osmotic flow of aqueous nanofluids through a microchannel with complex wave propagation using a

Buongiorno-type nanoscale model for nano-particle diffusion (species transfer). Prakash *et al.* [26] have investigated thermal radiation effects in nanoliquid flow induced by electroosmosis in tapered asymmetric channels with Brownian motion and thermophoretic body force effects. Sharma et al. [27] have examined the double diffusive convection in electroosmotic driven peristaltic pumping of nanofluids.

In above reviewed papers, most of the studies have addressed separately either thermophysical properties of the hybrid nanofluids or electroosmotic flow of nanofluids- however relatively few studies have examined simultaneously hybrid nanofluids in electro-osmotic peristaltic propulsion. In particular, an inspection of the literature has shown that thus far no study has focused on the peristaltic pumping of electroosmotic water-based hybrid nanofluids with three different types of metallic nanoparticles such as titania (TiO_2), alumina (Al_2O_3), and copper (Cu). This is the aim of the present work. Joule heating is also considered since it can be significant at larger voltages associated with reduction in flow rate and axial electro-osmotic current leakage and provides a more realistic simulation [28, 29]. Motivated by the modern research on hybrid nanotechnology, a new mathematical model is therefore formulated to simulate the flow, pumping and thermal characteristics for electroosmotic flow of three metallic/metallic oxide-aqueous nanofluids through an asymmetric microchannel with Joule dissipation, velocity/thermal slip and thermal buoyancy effects. The simulated results may be applicable in many biomedical and thermal systems to develop improved thermo-micro-pumping/chips, more efficient microchip cooling devices [30] as well as for applications involving micro-total analysis systems (μTAS) such as microfluidic reactors [31].

.

2. MATHEMATICAL MODEL

2.1. Flow regime

Consider the unsteady incompressible hybrid nanofluid, electro-osmotic flow induced by peristaltic propulsion through a two-dimensional asymmetric microchannel as exposed in **Fig.1**. An externally applied axial electric field and pressure gradient are present. The width of the channel is $d_1 + d_2$ and periodic flow is generated due to the sinusoidal wave trains propagating

with constant speed c along the deformable walls of the asymmetric microchannel. The shapes of the left and right walls are represented in the mathematical form given below:

$$\bar{h}_1\left(\bar{\xi},\bar{t}\right)=d_1+a_1\cos^2\left(\frac{\pi}{\lambda}\left(\bar{\xi}-c\bar{t}\right)\right), \tag{1}$$

$$\bar{h}_2\left(\bar{\xi},\bar{t}\right)=-d_2-a_2\cos^2\left(\frac{\pi}{\lambda}\left(\bar{\xi}-c\bar{t}\right)+\phi\right). \tag{2}$$

where a_1 and a_2 are wave amplitudes of right and left of wall, λ is the wavelength, ϕ $\left(0\le\phi\le\pi\right)$ is the variance of phase amongst the micro-channel walls that move sinusoidally.

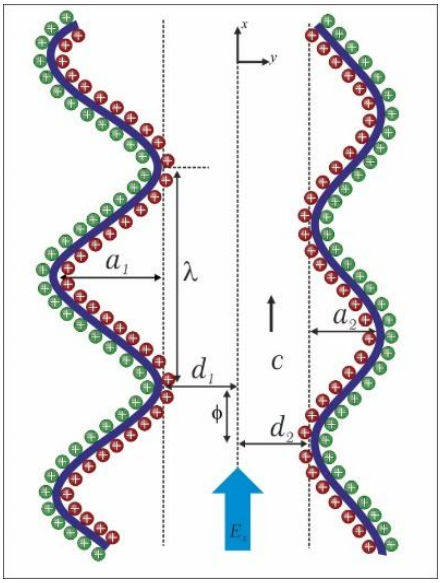

Fig.1. Schematic representation hybrid nanofluid flow through asymmetric channel

2.2. Governing equations

The appropriate conservation equations for mass, primary and secondary momentum and thermal energy are as follows:

$$\frac{\partial\bar{u}}{\partial\bar{\xi}}+\frac{\partial\bar{v}}{\partial\bar{\eta}}=0, \tag{3}$$

$$\rho_{eff}\left(\frac{\partial \bar{u}}{\partial \bar{t}}+\bar{u}\frac{\partial \bar{u}}{\partial \bar{\xi}}+\bar{v}\frac{\partial \bar{u}}{\partial \bar{\eta}}\right)=-\frac{\partial \bar{p}}{\partial \bar{\xi}}+\mu_{eff}\left(\frac{\partial^2 \bar{u}}{\partial \bar{\xi}^2}+\frac{\partial^2 \bar{v}}{\partial \bar{\eta}^2}\right)+\rho_e E_{\xi} + g\left(\left(1-\varpi\right)\rho_f\beta_f+\varpi\rho_p\beta_p\right)\left(\bar{T}-T_m\right), \tag{4}$$

$$\rho_{eff}\left(\frac{\partial \bar{v}}{\partial \bar{t}}+\bar{u}\frac{\partial \bar{v}}{\partial \bar{\xi}}+\bar{v}\frac{\partial \bar{v}}{\partial \bar{\eta}}\right)=-\frac{\partial \bar{p}}{\partial \bar{\eta}}+\mu_{eff}\left(\frac{\partial^2 \bar{v}}{\partial \bar{\xi}^2}+\frac{\partial^2 \bar{v}}{\partial \bar{\eta}^2}\right), \tag{5}$$

$$\left(\rho c\right)_{eff}\left(\frac{\partial \bar{T}}{\partial \bar{t}}+\bar{u}\frac{\partial \bar{T}}{\partial \bar{\xi}}+\bar{v}\frac{\partial \bar{T}}{\partial \bar{\eta}}\right)=\kappa_{eff}\left(\frac{\partial^2 \bar{T}}{\partial \bar{\xi}^2}+\frac{\partial^2 \bar{T}}{\partial \bar{\eta}^2}\right)+\mu_{eff}\left[2\left(\frac{\partial \bar{u}}{\partial \bar{\xi}}\right)^2+2\left(\frac{\partial \bar{v}}{\partial \bar{\eta}}\right)^2+\left(\frac{\partial \bar{u}}{\partial \bar{\eta}}+\frac{\partial \bar{v}}{\partial \bar{\xi}}\right)^2\right] + \sigma E_{\xi}^2. \tag{6}$$

where $\bar{u}$, $\bar{v}$ are the axial velocity components of $\bar{\xi}$ and $\bar{y}$ directions respectively, ρ_{eff}, $\bar{t}$, $\bar{p}$, μ_{eff}, σ, E_{ξ}, g, $\left(\rho\beta\right)_{eff}$, $T_m\left(=\frac{T_0+T_1}{2}\right)$, $\left(\rho c\right)_{eff}$, $\bar{T}$, κ_{eff} represent as the effective density, dimensional time, dimensional pressure, effective dynamic viscosity, electrical conductivity, axially-applied electric field strength, acceleration due to gravity, effective thermal expansion of the hybrid nanofluid, mean temperature, effective heat capacity, dimensional temperature and effective thermal conductivity.

In the present study, three different types of nanoparticles are considered with associated thermo-physical properties introduced in **Table -1**. It is observed from previous studies [32-34] that the single-phase nanofluid model may still be adopted as a reasonably accurate model for even hybrid nanoliquids. The appropriate relations for thermophysical properties are:

$$\rho_{eff}=\rho_f\left(1-\varpi\right)+\rho_p\varpi,\ \left(\rho c_p\right)_{eff}=\left(\rho c_p\right)_f\left(1-\varpi\right)+\left(\rho c_p\right)_p\varpi,\ \beta_{eff}=\beta_p\varpi+\beta_f\left(1-\varpi\right), \tag{7}$$

$$\mu_{eff}=\frac{\mu_f}{\left(1-\varpi\right)^{2.5}},\ \frac{\kappa_{eff}}{\kappa_f}=\frac{-2\varpi\left(\kappa_f-\kappa_p\right)+2\kappa_f+\kappa_p}{\varpi\left(\kappa_f-\kappa_p\right)+2\kappa_f+\kappa_p}. \tag{8}$$

in which ρ_f, ρ_p, ϖ, c_f, c_p, β_f, β_p, κ_f, κ_p and μ_f represent the density of fluid, density of nanoparticle, nanoparticle volume fraction, specific heat of fluid, specific heat of nanoparticle, fluid thermal expansion coefficient, nanoparticle thermal expansion coefficient, thermal

conductivity of fluid, thermal conductivity of nanoparticle and dynamic viscosity of fluid, respectively.

Table-1: Thermophysical properties of water and nanoparticles [32-34]

	ρ	c_p	κ	β
H_2O	997.1	4179	0.613	210
TiO_2	4250	686.2	8.9538	9
Al_2O_3	3970	765	40	8.5
Cu	8933	385	401	16.7

2.3. Electroosmotic fluid dynamics

According to the well-known Poisson equation, in the asymmetric microchannel, the electric potential $\bar{\Phi}$ is given by:

$$\nabla^2\bar{\Phi} = -\frac{\rho_e}{\varepsilon_{ef}}, \tag{9}$$

in which ε_{ef} is the dielectric constant and ρ_e is the net charge density of the electrolyte due to the presence of the electrical double layer (EDL) and it is given by:

$$\rho_e = ez\left(\bar{n}_+ - \bar{n}_-\right), \tag{10}$$

where e is the electronic charge, z is the charge balance, $\bar{n}_+$ and $\bar{n}_-$ represent positive and negative ions having bulk concentration, respectively.

2.4. Governing equations in wave frame

In view of a wave frame (ξ', η') that passes with a velocity *c* away from the fixed frame $\left(\bar{\xi}, \bar{\eta}\right)$, we write:

$$\xi' = \bar{\xi} - c\bar{t},\ \eta' = \bar{\eta},\ u' = \bar{u} - c,\ v' = \bar{v},\ \ p' = \bar{p},\ T' = \bar{T}. \tag{11}$$

The transformed conservation Eqns. (3)-(6) in the wave frame emerge as:

$$\frac{\partial u'}{\partial \xi'}+\frac{\partial v'}{\partial \eta'}=0, \tag{12}$$

$$\left(\left(1-\varpi\right)\rho_f+\varpi\rho_p\right)\left(\left(u'+c\right)\frac{\partial u'}{\partial \xi'}+v'\frac{\partial u'}{\partial \eta'}\right)=-\frac{\partial p'}{\partial \xi'}+\frac{\mu_f}{\left(1-\varpi\right)^{2.5}}\left(\frac{\partial^2 u'}{\partial \xi'^2}+\frac{\partial^2 v'}{\partial \eta'^2}\right) + \rho_e E_\xi + g\left(\left(1-\varpi\right)\rho_f\beta_f+\varpi\rho_p\beta_p\right)\left(T'-T_m\right), \tag{13}$$

$$\left(\left(1-\varpi\right)\rho_f+\varpi\rho_p\right)\left(\left(u'+c\right)\frac{\partial v'}{\partial \xi'}+v'\frac{\partial v'}{\partial \eta'}\right)=-\frac{\partial p'}{\partial \eta'}+\frac{\mu_f}{\left(1-\varpi\right)^{2.5}}\left(\frac{\partial^2 v'}{\partial \xi'^2}+\frac{\partial^2 v'}{\partial \eta'^2}\right), \tag{14}$$

$$\begin{aligned}&\left(\left(1-\varpi\right)\left(\rho c\right)_f+\varpi\left(\rho c\right)_p\right)_{eff}\left(\left(u'+c\right)\frac{\partial T'}{\partial \xi'}+v'\frac{\partial T'}{\partial \eta'}\right)\\&=\kappa_f\kappa_1\left(\frac{\partial^2 T'}{\partial \xi'^2}+\frac{\partial^2 T'}{\partial \eta'^2}\right)+\frac{\mu_f}{\left(1-\varpi\right)^{2.5}}\left[2\left(\frac{\partial u'}{\partial \xi'}\right)^2+2\left(\frac{\partial v'}{\partial \eta'}\right)^2+\left(\frac{\partial u'}{\partial \eta'}+\frac{\partial v'}{\partial \xi'}\right)^2\right]+\sigma E_\xi^2.\end{aligned} \tag{15}$$

2.5. Non-dimensional analysis and approximations

The following dimensionless variables are introduced:

$$\xi=\frac{\xi'}{\lambda},\eta=\frac{\eta'}{d_1},u=\frac{u'}{c},v=\frac{v'}{c\delta},\delta=\frac{d_1}{\lambda},h_1=\frac{\bar{h}_1}{d_1},h_2=\frac{\bar{h}_2}{d_1},d=\frac{d_2}{d_1},a=\frac{a_1}{d_1},b=\frac{a_2}{d_1},p=\frac{d_1^2 p'}{c\lambda\mu_f},$$

$$\theta=\frac{T'-T_m}{T_1-T_0},\mathrm{Re}=\frac{\rho_f c d_1}{\mu_f},\mathrm{Pr}=\frac{\mu_f c_f}{\kappa_f},Ec=\frac{c^2}{c_f\left(T_1-T_0\right)},Br=\mathrm{Pr}\,Ec,\Phi=\frac{\bar{\Phi}}{\tilde{\xi}},$$

$$\gamma=\frac{\sigma d_1^2 E_\xi^2}{\kappa_f\left(T_1-T_0\right)},Uhs=-\frac{E_\xi\varepsilon\tilde{\xi}}{c\mu_f},Gr=\frac{g\rho_f\beta_f\left(T_1-T_0\right)d_1^2}{c\mu_f},u=\frac{\partial\psi}{\partial\eta},v=-\frac{\partial\psi}{\partial\xi}. \tag{16}$$

The electric charge density follows the Boltzmann distribution which is given by:

$$\rho_e=-2n_0 ez\sinh\left(\frac{ez\bar{\Phi}}{k_B T_n}\right), \tag{17}$$

where n_0, e, z, k_B and T_n represent the bulk concentration (number density), elementary charge valence, Boltzmann constant and absolute temperature. Using Debye-Hückel linearization, the Poisson-Boltzmann equation reduces to:

$$\nabla^2\bar{\Phi} = \kappa^2\bar{\Phi}, \tag{18}$$

Here $\kappa = d_1 ez\sqrt{\frac{2n_0}{\varepsilon k_B T}}$, represents the *ratio of the characteristic transverse length to the Debye length* (electroosmosis parameter); this indicates the penetration of the zeta potential at the surface into the bulk hybrid nanofluid. Utilizing Debye-Hückel linearization again, the non-dimensional Poisson-Boltzmann equation with lubrication approximations, effectively Eqns. (12)-(15) and (18), assume the form:

$$\frac{\partial p}{\partial \xi} = A_1\frac{\partial^3 \psi}{\partial \eta^3} + A_2 Gr\theta + \kappa^2 Uhs\Phi, \tag{19}$$

$$\frac{\partial p}{\partial \eta} = 0, \tag{20}$$

$$\frac{\partial^2 \Phi}{\partial \eta^2} = \kappa^2\Phi, \tag{21}$$

$$\kappa_1\frac{\partial^2\theta}{\partial\eta^2} + BrA_1\left(\frac{\partial^2\psi}{\partial\eta^2}\right)^2 + \gamma = 0. \tag{22}$$

Elimination of the axial and transverse pressure gradient terms from Eqns. (20) and (21), yields:

$$A_1\frac{\partial^4\psi}{\partial y^4} + A_2 Gr\frac{\partial\theta}{\partial y} + \kappa^2 Uhs\frac{\partial\Phi}{\partial y} = 0. \tag{23}$$

in which a and b denote the dimensionless amplitudes at the microchannel walls (h_1 and h_2 respectively for the left wall and right wall), while δ, Re, p, Gr, Pr, Ec, Br, Uhs, γ and ψ represent the wave number, Reynolds number, dimensionless pressure, thermal Grashof number, Prandtl number, Eckert number, Brinkman number, Helmholtz-Smoluchowski (electro-osmotic) velocity, Joule-heating parameter and dimensionless stream function respectively. The coefficients A_1, A_2 and κ_1 have constant values and are given by:

$$A_1 = \frac{1}{(1-\varpi)^{2.5}},\ A_2 = 1-\varpi+\varpi\left(\frac{(\rho\beta)_p}{(\rho\beta)_f}\right),\ \kappa_1 = \frac{-2\varpi(\kappa_f-\kappa_p)+2\kappa_f+\kappa_p}{\varpi(\kappa_f-\kappa_p)+2\kappa_f+\kappa_p}. \tag{24}$$

2.6. Flow rate analysis

The dimensional volumetric flow rate in the *laboratory frame* is:

$$Q = \int_{\bar{h}_2(\bar{\xi},\bar{t})}^{\bar{h}_1(\bar{\xi},\bar{t})} \bar{u}(\bar{\xi},\bar{\eta},t)d\bar{\eta}, \tag{25}$$

The volumetric flow rate in the wave frame is given by:

$$q = \int_{h_2(\xi')}^{h_1(\xi')} u'(\xi',\eta')d\eta', \tag{26}$$

which, on integration of Eqn. (26), yields:

$$q = Q + h_1 - h_2 . \tag{27}$$

Averaging the volumetric flow rate along one time period (27), we get:

$$\Theta = \int_0^1 Q \quad dt = \int_0^1 (q + h_2 - h_1) \quad dt, \tag{28}$$

which yields:

$$\Theta = q + 1 + d + \left(\frac{a+b}{2}\right). \tag{29}$$

2.7. Boundary conditions and analytical solution

The non-dimensional boundary conditions for the system are prescribed, following [32-34] as:

$$\psi = \frac{q}{2}, \frac{\partial \psi}{\partial \eta} + \frac{\xi_1}{(1-\varpi)^{2.5}} \frac{\partial^2 \psi}{\partial \eta^2} = -1, \theta + \xi_2 \frac{\partial \theta}{\partial \eta} = -\frac{1}{2} \text{ and } \Phi = 1 \text{ at } y = h_1, \tag{30}$$

$$\psi = -\frac{q}{2}, \frac{\partial \psi}{\partial \eta} - \frac{\xi_1}{(1-\varpi)^{2.5}} \frac{\partial^2 \psi}{\partial \eta^2} = -1, \theta - \xi_2 \frac{\partial \theta}{\partial \eta} = \frac{1}{2} \text{ and } \Phi = 0 \text{ at } y = h_2 . \tag{31}$$

Here ξ_1 and ξ_2 are respectively *the dimensionless axial velocity slip* and *thermal slip* parameters. The no-slip case can be retrieved as a limiting case of the general model by setting $\xi_1 = \xi_2 = 0$.

Also, shapes of walls in non-dimensional form are now defined as:

$$h_1(\xi) = 1 + a\cos^2(\pi\xi), \tag{32}$$

$$h_2(\xi) = -d - b\cos^2(\pi\xi + \phi). \tag{33}$$

3. NUMERICAL SOLUTION WITH MATLAB BVP4C SOLVER

The governing equations (21)-(23) are coupled non-linear ordinary differential equations with the associated boundary conditions given in equations (30)-(31). This boundary value problem is solved numerically by using the symbolic computer algebra software MATLAB bvp4c routine. The non-linear coupled ordinary differential equations are converted into a set of first order ordinary differential equations as follows:

$$\left.\begin{aligned}
&\psi = y_1; \quad \frac{\partial\psi}{\partial\eta} = y_2; \quad \frac{\partial^2\psi}{\partial\eta^2} = y_3; \quad \frac{\partial^3\psi}{\partial\eta^3} = y_4;\\
&\frac{\partial^4\psi}{\partial\eta^4} = \frac{-1}{A_1}\left(A_2 Gr\, y_6 + \kappa^2 Uhs\, y_8\right);\\
&\theta = y_5; \quad \frac{\partial\theta}{\partial\eta} = y_6; \quad \frac{\partial^2\theta}{\partial\eta^2} = \frac{-1}{\kappa_1}\left(\gamma + BrA_1\left(y_3\right)^2\right);\\
&\Phi = y_7; \quad \frac{\partial\Phi}{\partial\eta} = y_8; \quad \frac{\partial^2\Phi}{\partial\eta^2} = \kappa^2 y_7;
\end{aligned}\right\} \tag{34}$$

The corresponding boundary condition (30) and (31) can be written as:

$$y_1(h_1) = \frac{q}{2};\ y_2(h_1) + \frac{\xi_1}{(1-\varpi)^{2.5}}\, y_3(h_1) = -1;\ y_5(h_1) + \xi_2 y_6(h_1) = -0.5;\ y_7(h_1) = 1; \tag{35a}$$

$$y_1(h_2) = -\frac{q}{2};\ y_2(h_2) - \frac{\xi_1}{(1-\varpi)^{2.5}}\, y_3(h_2) = -1;\ y_5(h_2) - \xi_2 y_6(h_2) = 0.5;\ y_7(h_2) = 0; \tag{35b}$$

The absolute and relative errors of tolerance on the residuals are set by

$$options = bvpset\left("AbsTol", le-10, 'RelTol', le-10\right) \tag{36}$$

Initial value problems are resolved by "$bvpinit$"

$$sol\,\text{in}\,it = bvpinit\left(linspace\left(0,10,50\right),\left[0,10\right]\right). \tag{37}$$

The subsequent code implemented the boundary value problem along with corresponding boundary conditions as:

$$sol = bvp4c\left(\,file\_ode,\, file\_bc, solinit, options\right) \tag{38}$$

4. NUMERICAL RESULTS AND DISCUSSION

The numerical solutions are discussed through an exhausting of three different type of nanofluid with water as the base fluid for alumina $\left(Al_2O_3\right)$, copper $\left(Cu\right)$ and titania $\left(TiO_2\right)$. In **Table 1** relevant values are given for the nanoliquid properties. To elucidate the impact of different electrical, thermal and nanoscale parameters, an extensive number of graphs have been produced for axial velocity, pressure gradient and temperature distributions in the asymmetric microchannel and are depicted in **Figs. 2-23**. **Fig. 2** clearly visualizes the effective thermal conductivity of the water based nanofluid with varying nanoparticle volume fraction behavior based on the Maxwell model (described earlier) and the three different types of metallic nanoparticles i.e. alumina $\left(Al_2O_3\right)$, titania $\left(TiO_2\right)$ and copper $\left(Cu\right)$ nanofluid with water as the base liquid. It is evident that the *Cu-water nanofluid* achieves the best and most consistent thermal conductivity enhancement at any value of nano-particle volume fraction (ϖ, see Eqn. (8)). Although there is also an increase for alumina and titania, there is pronounced deviation at maximum volume fraction (0.5). Alumina however produces more enhancement than titania at any volume fraction. It is also clearly observed that a *non-linear (montonic growth) relation* exists between thermal conductivity ratio and volume fraction for water-based metallic nanofluids.

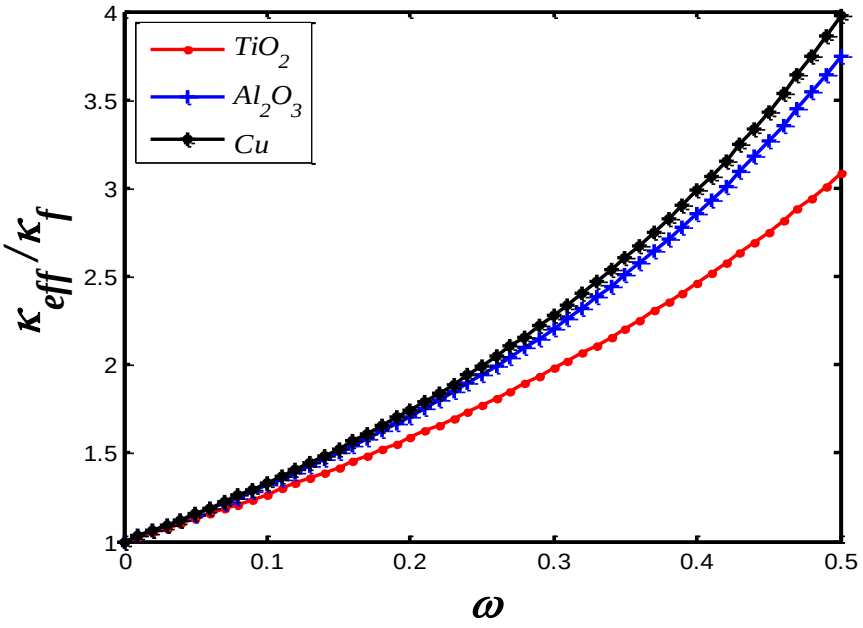

Fig.2 The relation between effective thermal conductivity to thermal conductivity ratio and nano-particle volume fraction for water based metallic nanofluid

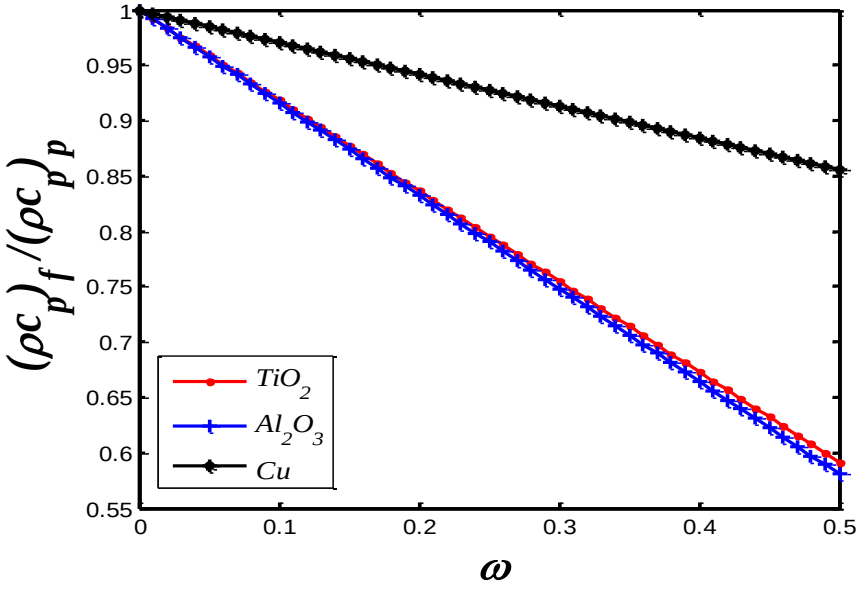

Fig.3 The relation between effective heat capacity and heat capacity ratio and volume fraction for water based metallic nanofluid

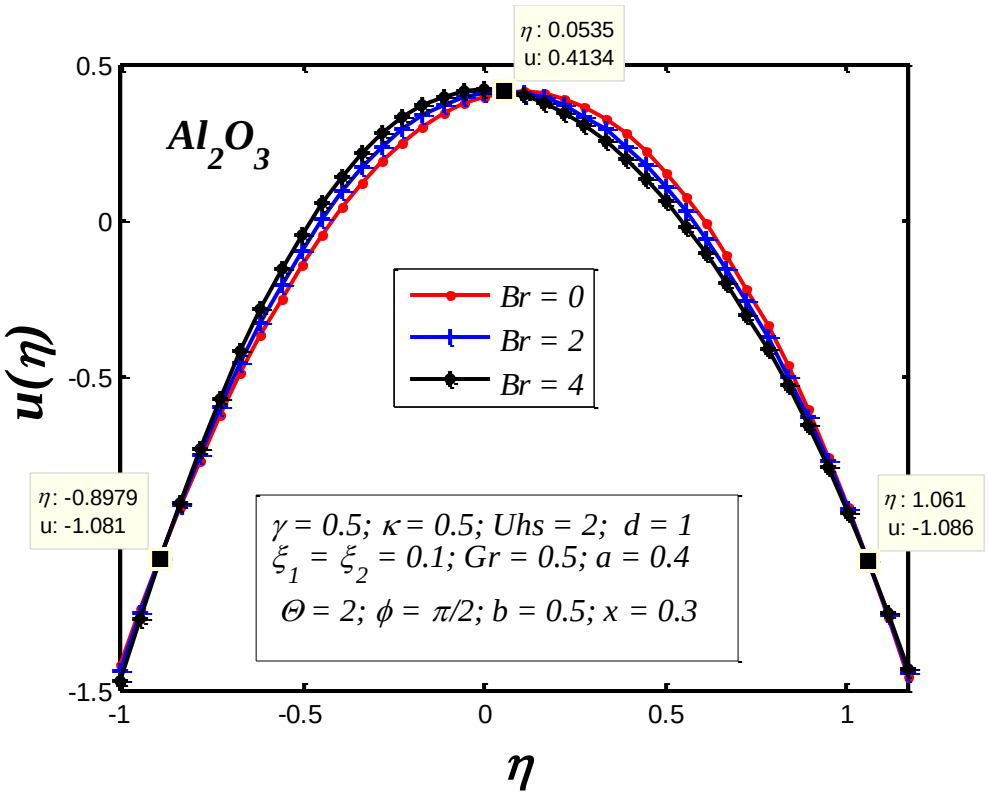

Fig.4 The impact of Brinkman number Br on axial velocity for $Al_2O_3 - H_2O$ nanofluid

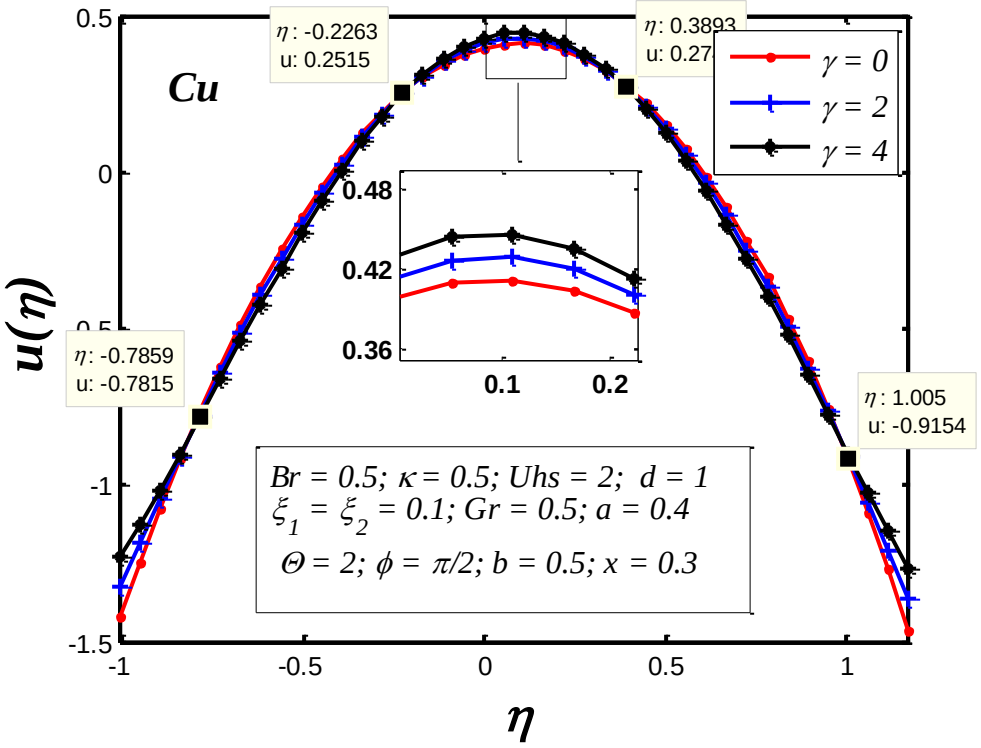

Fig.5 The impact of Joule parameter, γ on axial velocity distribution for $Cu - H_2O$ nanofluid

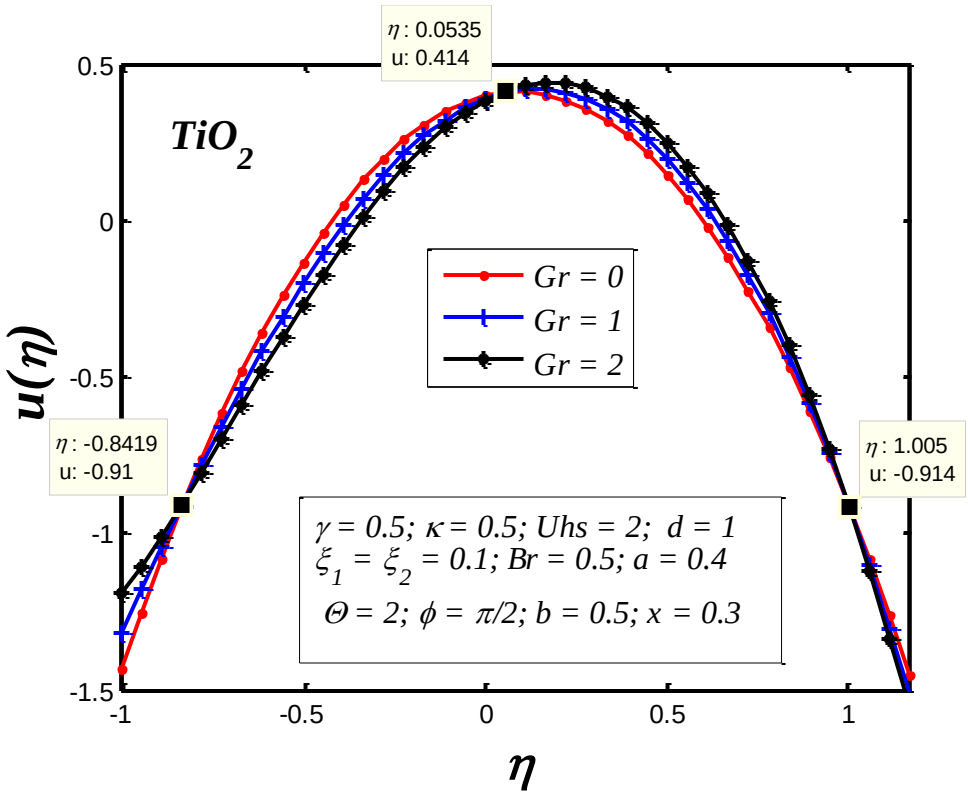

Fig.6 The impact of thermal Grashof number Gr on axial velocity for $TiO_2 - H_2O$ nanofluid

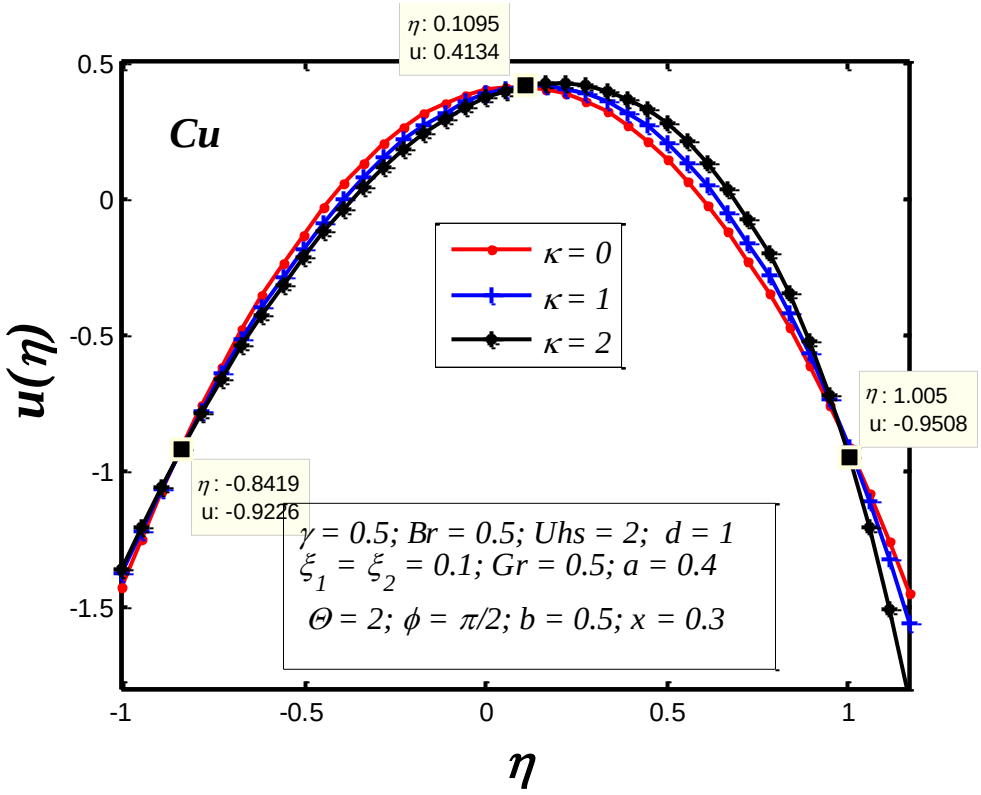

Fig.7 The impact of inverse Debye parameter κ on axial velocity for $Cu - H_2O$ nanofluid

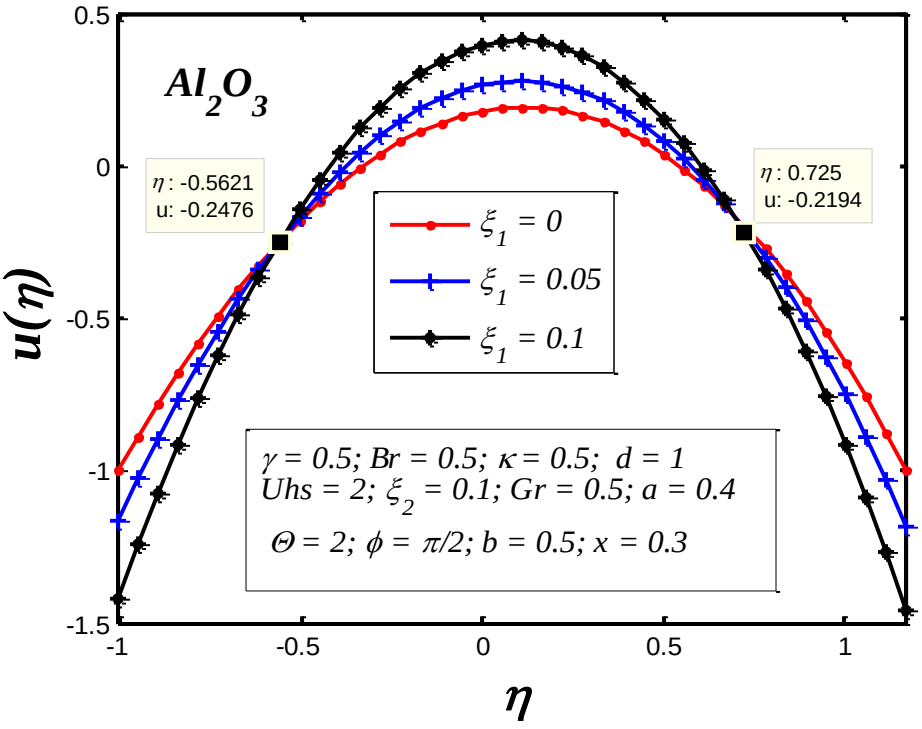

Fig.8 The impact of velocity slip (ξ_1) on axial velocity distribution for $Al_2O_3 - H_2O$ nanofluid

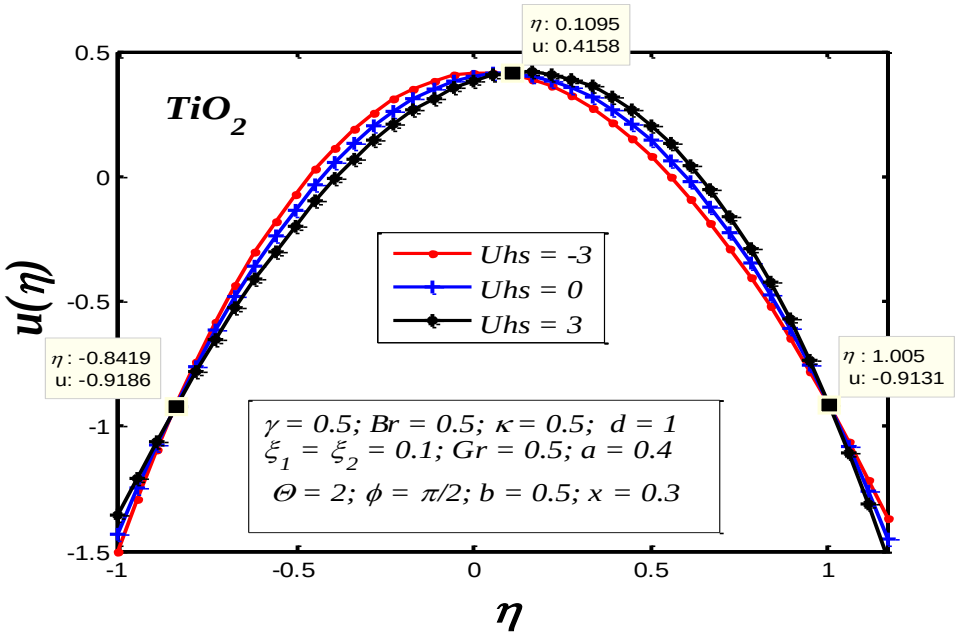

Fig.9 The impact of electro-osmotic velocity (*Uhs*) on axial velocity for $TiO_2 - H_2O$ nanofluid

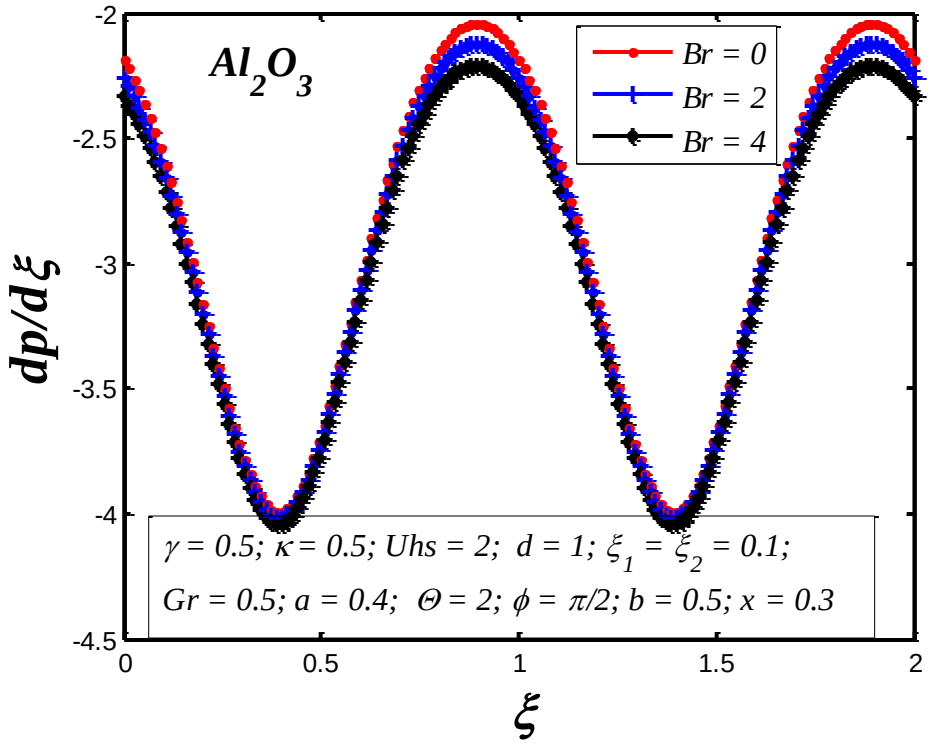

Fig.10 The impact of Br on pressure gradient distribution for $Al_2O_3 - H_2O$ nanofluid

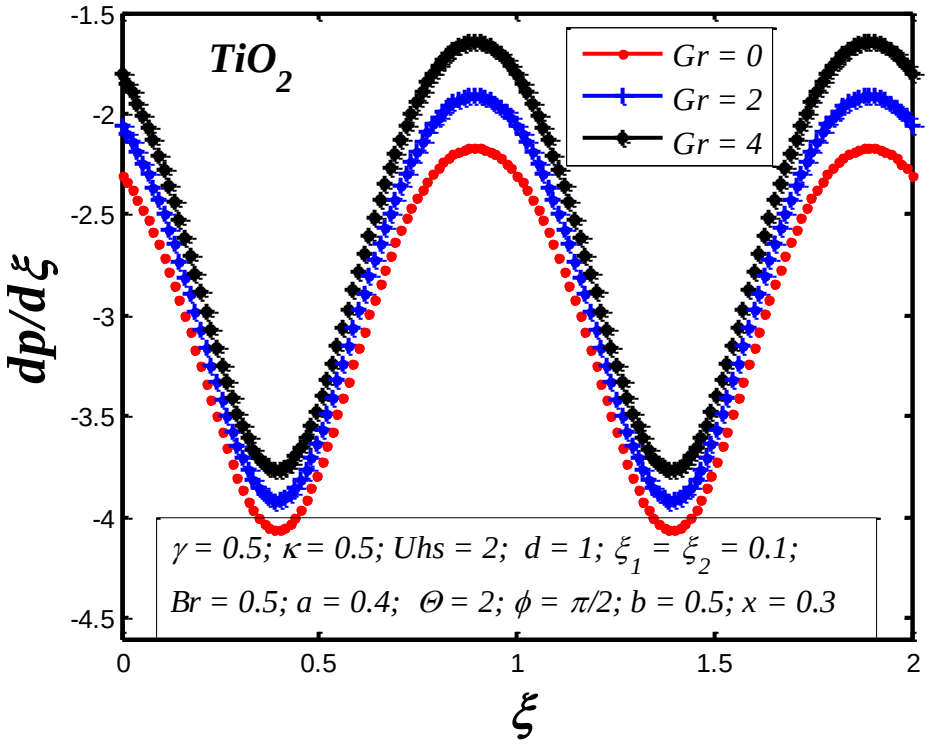

Fig.11 The impact of Gr on pressure gradient distribution for $TiO_2 - H_2O$ nanofluid

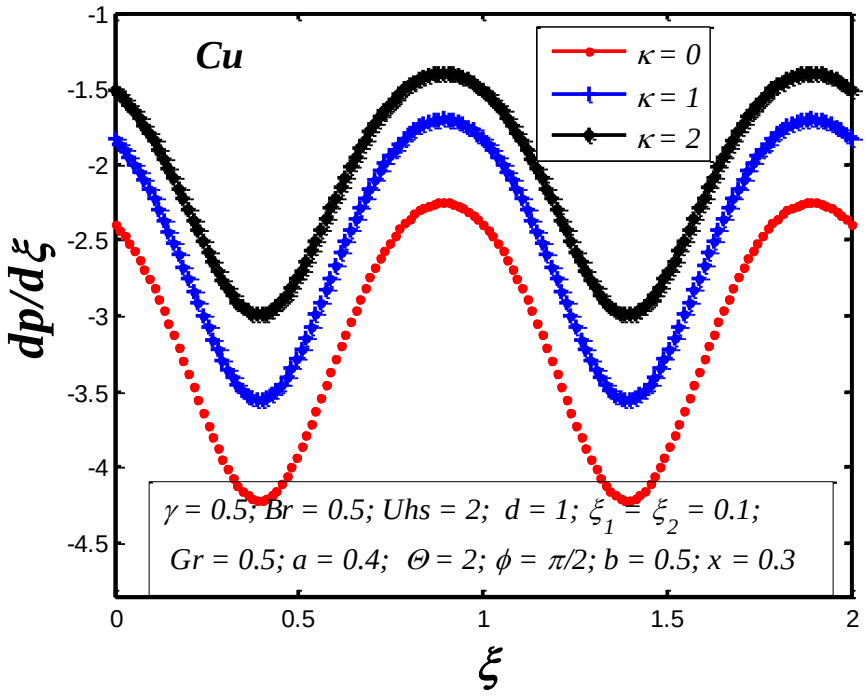

Fig.12 The impact of κ on pressure gradient distribution for $Cu-H_2O$ nanofluid

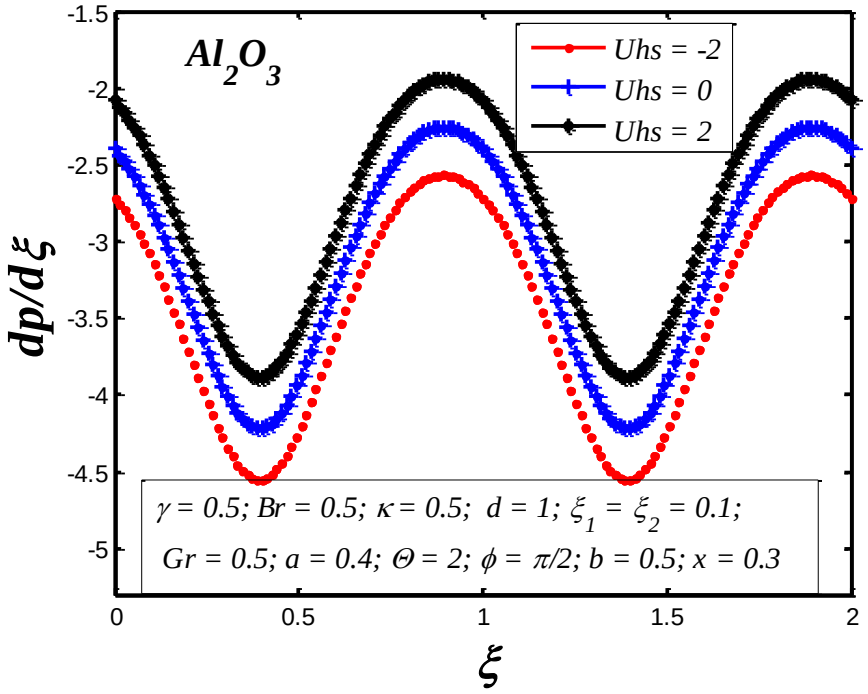

Fig.13 The impact of Uhs on pressure gradient distribution for $Al_2O_3-H_2O$ nanofluid

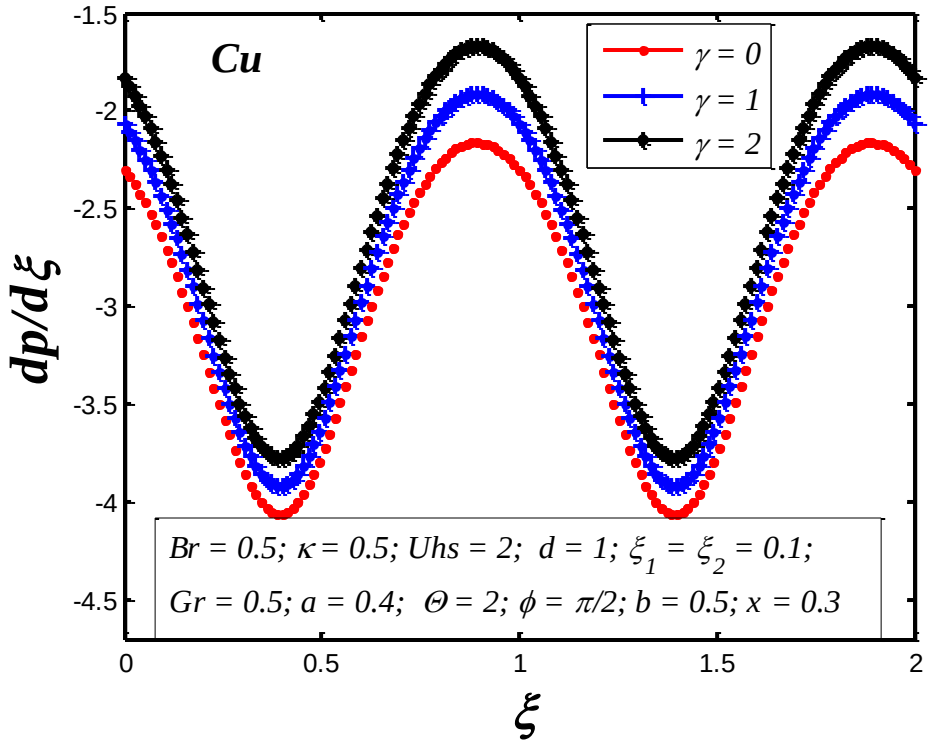

Fig.14 The impact of γ on pressure gradient distribution for $Cu-H_2O$ nanofluid

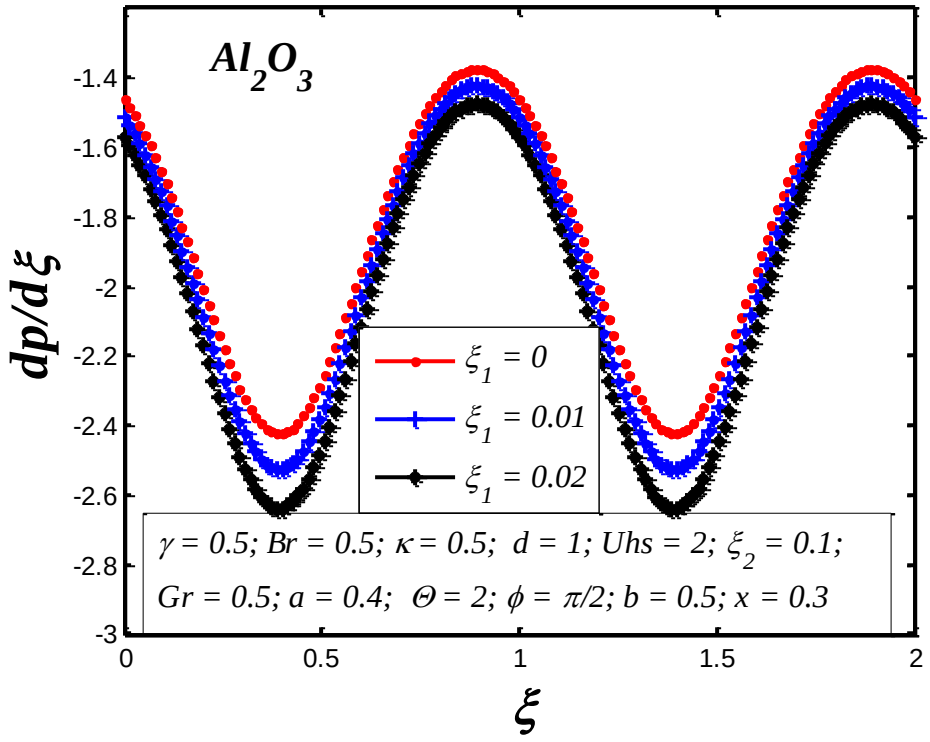

Fig.15 The impact of ξ_1 on pressure gradient distribution for $Al_2O_3-H_2O$ nanofluid

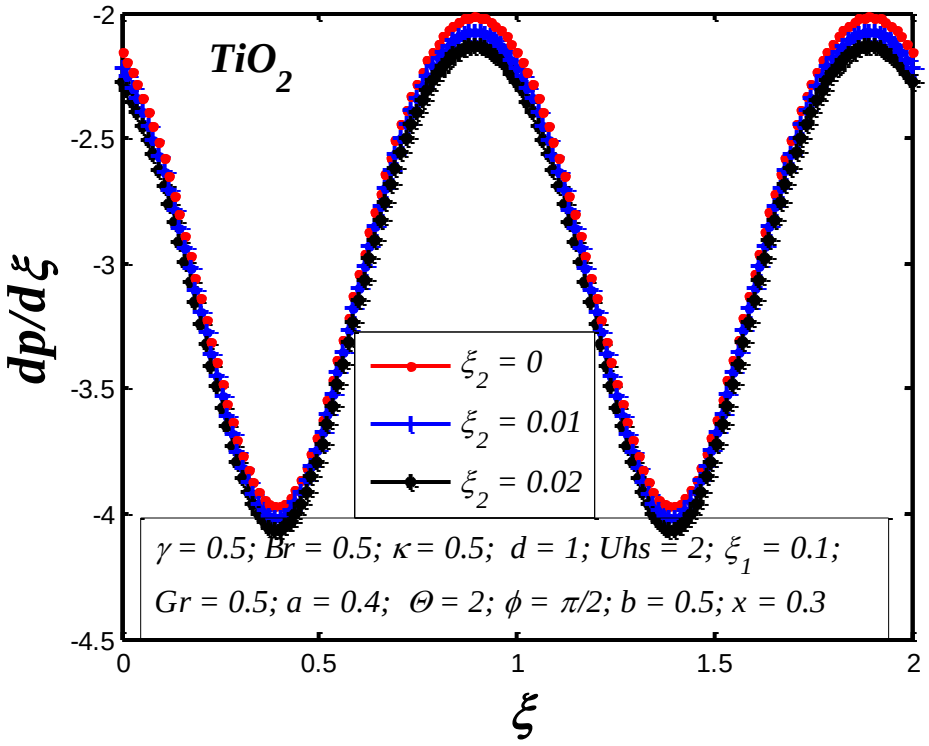

Fig.16 The impact of ξ_2 on pressure gradient distribution for $TiO_2 - H_2O$ nanofluid

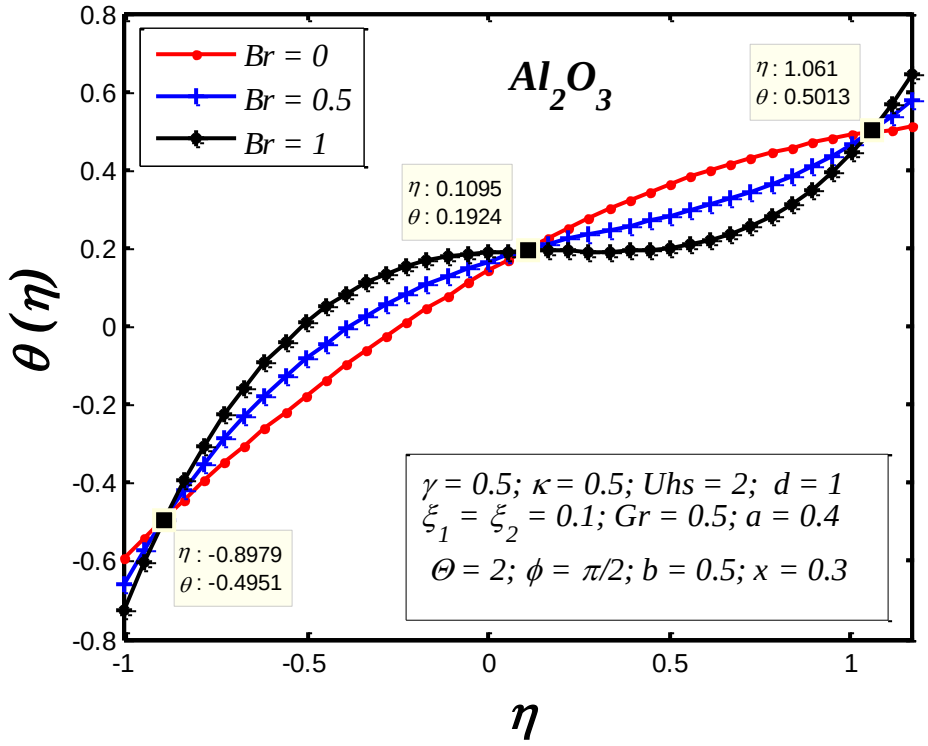

Fig.17 The impact of Br on temperature distribution for $Al_2O_3 - H_2O$ nanofluid

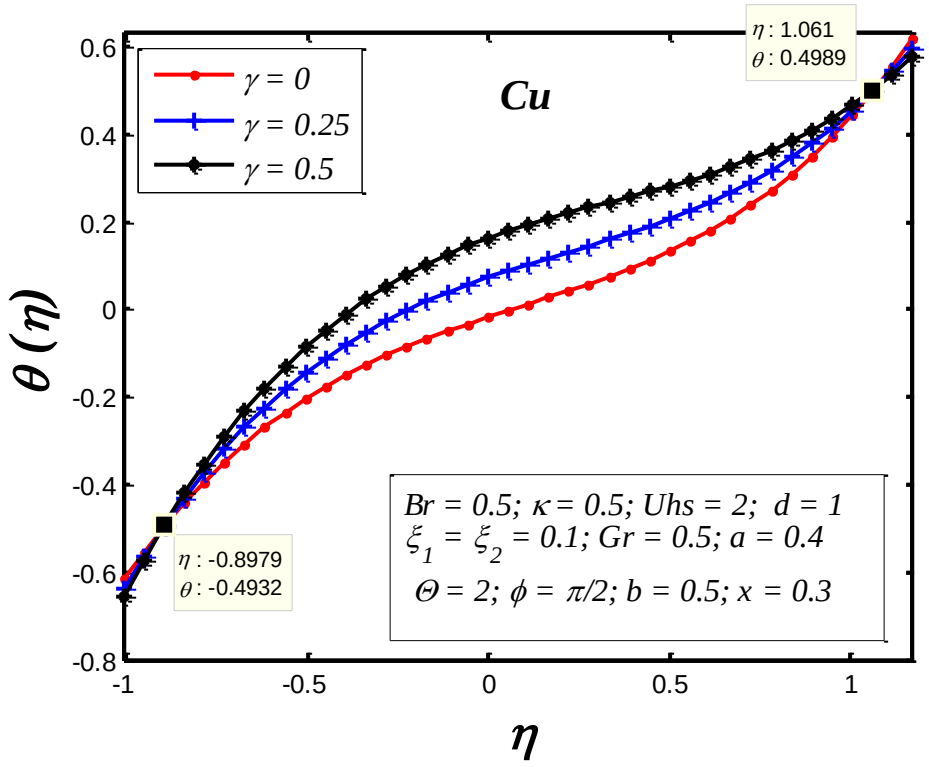

Fig.18 The impact of γ on temperature distribution for $Cu-H_2O$ nanofluid

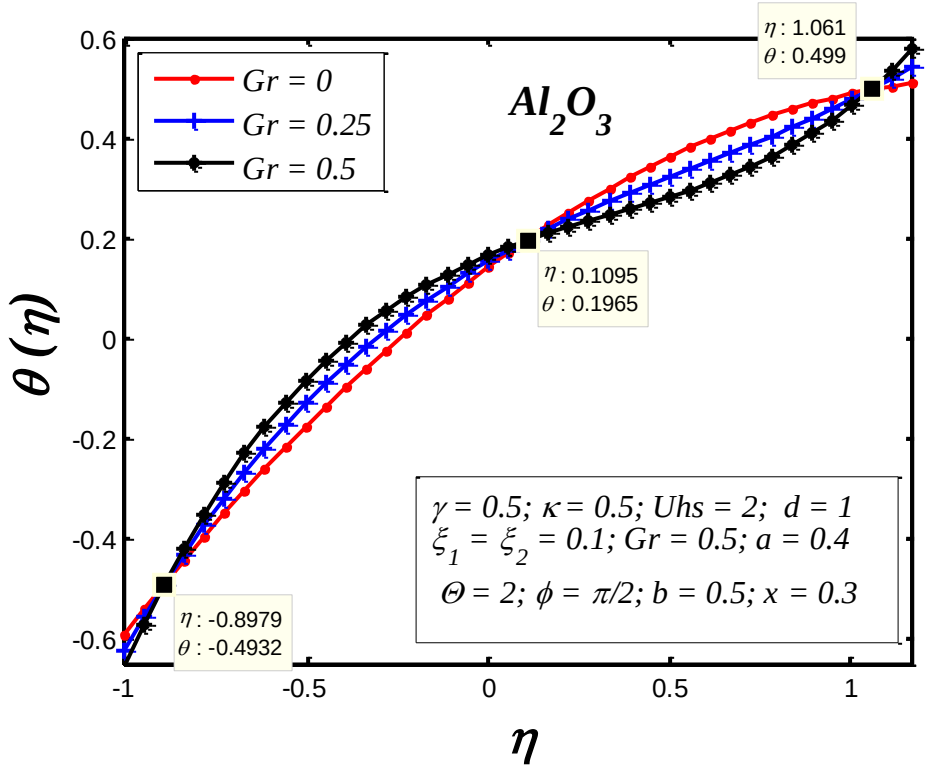

Fig.19 The impact of Gr on temperature distribution for $Al_2O_3-H_2O$ nanofluid

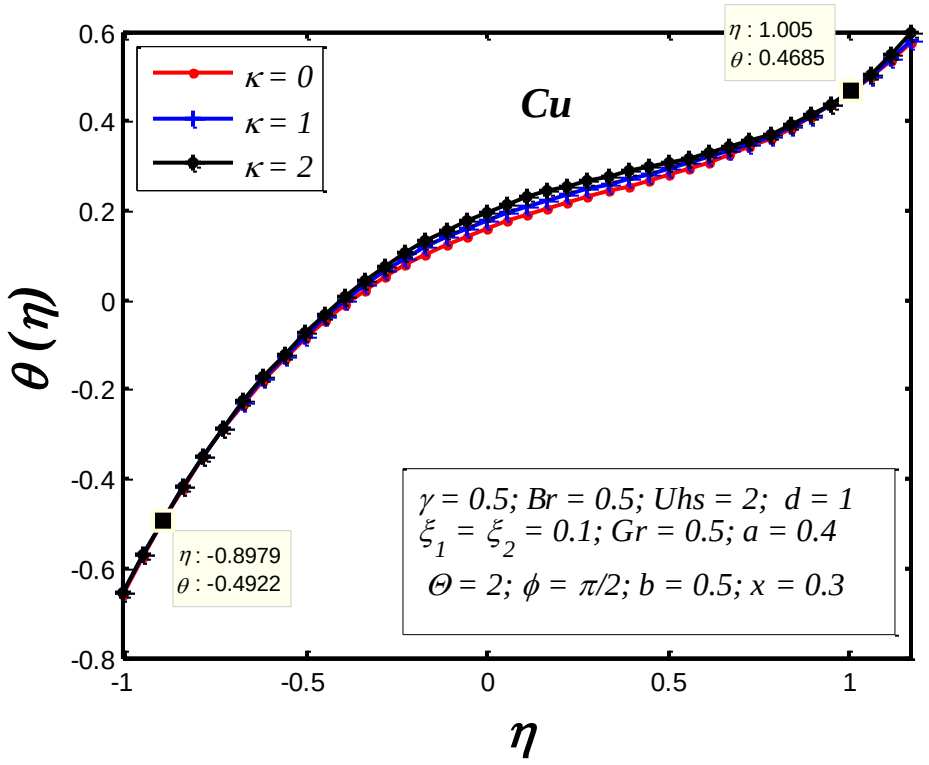

Fig.20 The impact of κ on temperature distribution for $Cu-H_2O$ nanofluid

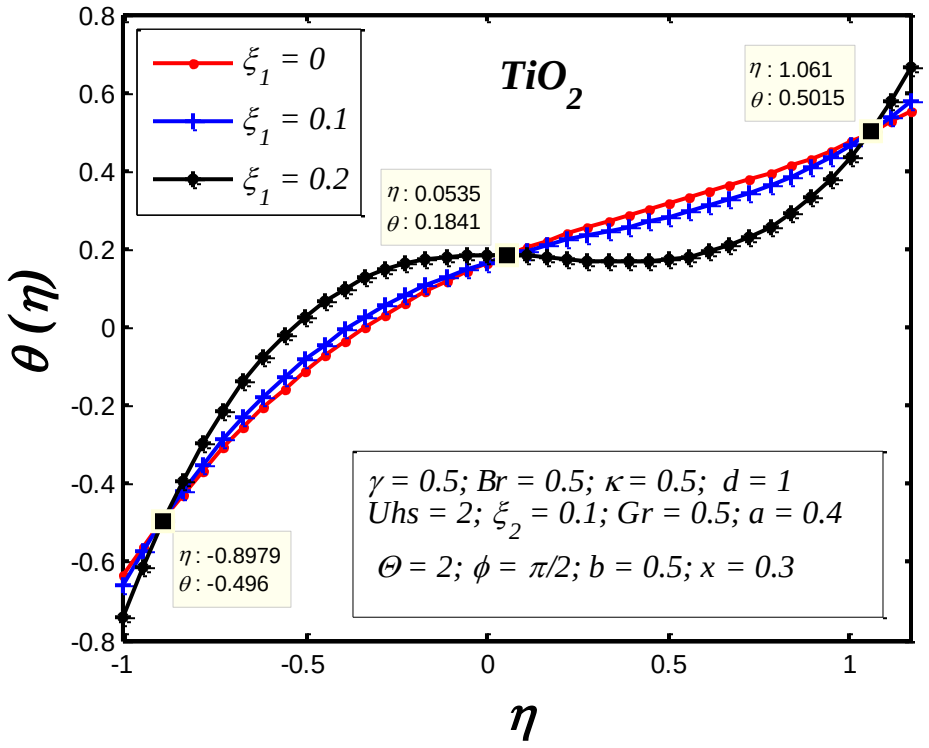

Fig.21 The impact of ξ_1 on temperature distribution for TiO_2-H_2O nanofluid

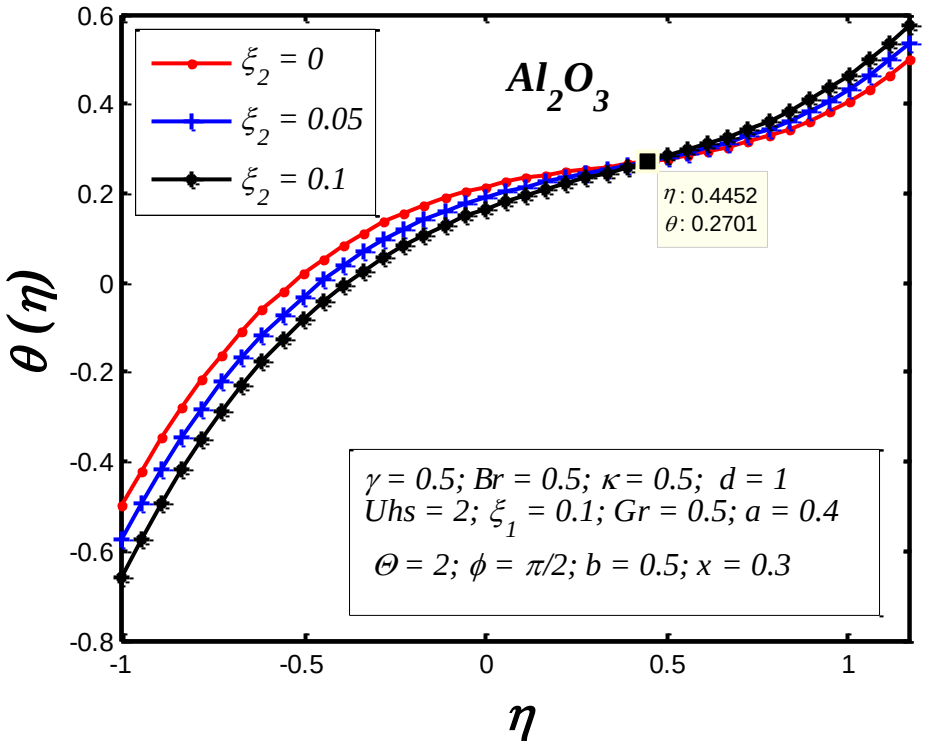

Fig.22 The impact of ξ_2 on temperature distribution for $Al_2O_3 - H_2O$ nanofluid

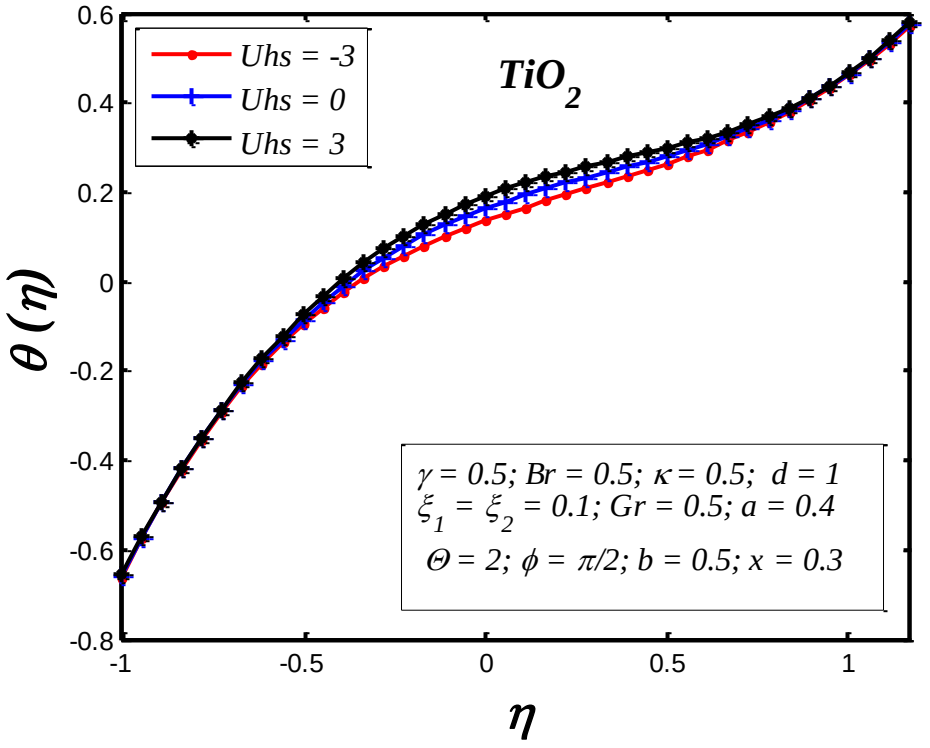

Fig.23 The impact of Uhs on temperature distribution for $TiO_2 - H_2O$ nanofluid

In **Fig.3** illustrates the evolution of ratio of effective heat capacity and heat capacity i.e. $(\rho c_p)_f/(\rho c_p)_p$ with nanoparticle volume fraction (ϖ) for metallic water-based nanofluid. There is evidently a linear decay relationship observed i.e. with increasing nanoparticle volume fraction (ϖ), there is a strong reduction in heat capacity ratio. The highest heat capacity is attained for copper, (*Cu*) owing to superior thermal conductivity of copper nano-particles, and this is significantly greater than alumina (Al_2O_3) and titania (TiO_2). The heat capacity of alumina (Al_2O_3) is marginally lower than titania (TiO_2). These results concur with many other studies including Minea [5] (who considered hybrid nanofluids based on Al_2O_3, TiO_2 and SiO_2) and also Kuharat and Bég [7] who examined all three metallic nanoliquids i.e. Al_2O_3, TiO_2 and Cu-water, although they considered 3-dimensional forced convection in the absence of electro-osmotic and peristaltic effects).

3.1 Axial velocity distribution

Figs.4-9 depict the respective influences of Brinkman number (Br), Joule-heating parameter (γ), thermal Grashof number (Gr), electro-osmosis parameter (κ), axial velocity slip parameter (ξ_1) *and* Helmholtz-Smoluchowski (electro-osmotic) velocity (Uhs) for fixed value of the nanoparticle volume fraction ($\varpi = 0.1$). **Fig. 4** depicts the impact of Brinkman parameter Br on the axial velocity field for water base alumina nanofluid. It is noticed that an increase in Br (corresponding to stronger viscous dissipation) elevates the axial velocity of nanoliquid in the left half space of the microchannel but depletes it in the right half space. The case of non-dissipative flow corresponds to $Br = 0$. Evidently inclusion of viscous dissipation is non-trivial and the results show that its neglection in mathematical models leads to either under or over-predictions in velocity magnitudes. **Fig.5** illustrates that with an increase of Joule-heating parameter, the axial velocity field decreases in the core part of the microchannel for water based titania nanofluid whereas it is weakly elevated in the peripheral zones (near the left and right walls). These results correspond to the axially aligned electrical field case i.e. where E_ξ is in the positive ξ-direction. Clearly Joule dissipation does not exert the same effect across the micro-channel width as also noted in [28, 29]. **Fig. 6** reveals that with increasing thermal Grashof number (*Gr)* axial velocity (for water-based copper nanofluid) varies in response from the left wall to the right wall. Initially acceleration is

induced at the left wall and thereafter deceleration towards the central line of the microchannel; however, in the right half space again acceleration is caused in the axial flow. The case $Gr = 0$ corresponds to forced convection. **Fig. 7** shows the effects of electroosmosis parameter (inverse Debye length parameter, $\kappa = d_1 ez\sqrt{\frac{2n_0}{\varepsilon k_B T}}$) on axial velocity distribution for water base copper nanofluid. Significant flow deceleration is instigated in the left half space whereas acceleration in the axial flow is induced in the right half space of the microchannel. Therefore, with lower Debye lengths (higher electro-osmotic parameter, κ) both acceleration and deceleration can be generated in different sections of the micro-channel. The effect of slip axial velocity on axial velocity distribution for water-based alumina nanofluid is shown in **Fig. 8.** Evidently increasing ξ_1 accelerates the axial velocity in the core part of the microchannel whereas it decelerates the flow at the microchannel walls and near the walls. The influence of Helmholtz-Smoluchowski velocity (U_{hs}) on axial velocity for water based titania nanofluid is shown in **Fig.9.** It is apparent that axial velocity of the hybrid nanofluid increases over the ranges $\left(h_1 \le \eta \le -0.8419\right)$ and $\left(0.1095 \le \eta \le 1.005\right)$ whereas the reverse effect i.e. deceleration is generated in the other sections of the channel. Negative values of $Uhs = -\frac{E_\xi \varepsilon \tilde{\xi}}{c\mu_f}$ imply that the axial electrical field E_ξ is in the positive ξ-direction whereas positive values correspond to a reversal in the axial field direction. Electro-osmotic effects are negated for $U_{hs} = 0$. Evidently the axial flow is very sensitive to the direction of the applied electrical field and orientation of the electrical field can therefore be utilized to induce either acceleration or retardation in hybrid aqueous nanofluids, as noted in [30] and [31].

3.2 Pressure gradient distribution

Axial pressure gradient $\left(dp/d\xi\right)$ is calculated by using the relationship, $\frac{\partial p}{\partial \xi} = A_1 \frac{\partial^3 \psi}{\partial \eta^3} + A_2 Gr\theta + \kappa^2 Uhs\Phi,$ over two oscillating periods for the peristaltic wave. The visual representation of the relations between the axial pressure gradient distribution $\left(dp/d\xi\right)$ and axial coordinate $\left(\xi\right)$ are shown in **Figs. 10-16** for different values of $Br,\ Gr,\ \kappa,\ Uhs,\ \gamma,\ \xi_1$ and ξ_2 for water based nanoliquid doped with three different types of the nanoparticles i.e. titania $\left(TiO_2\right)$,

alumina $\left(Al_2O_3\right)$ and copper $\left(Cu\right)$. The periodic (oscillatory) nature of the pressure gradient variation along the microchannel length is clearly captured in all the figures due to the sinusoidal peristaltic waves propagating along the microchannel walls. The nanoparticle volume fraction value is fixed as $\varpi = 0.1$. The influence of alumina-water nanofluid of the Brinkman number on pressure gradient is presented in **Fig.10.** Generally, pressure gradient is reduced with increasing Brinkman number. In the absence of viscous dissipation (*Br* = 0) maximum magnitudes of axial pressure gradient are computed. In **Fig.11**, we observed that with increasing thermal Grashof number for titania-water nanofluid, axial pressure gradient is consistently enhanced uniformly along the microchannel. Clearly an accentuation in thermal buoyance force i.e. higher *Gr*, encourages axial pressure gradient development and leads to more efficient pumping. The influence of electro-osmosis parameter $\left(\kappa\right)$ on pressure gradient for water-based copper is presented in **Fig. 12.** It is found that with higher values of κ, i.e. lower Debye lengths, there is a substantial elevation in pressure gradient magnitudes along the entire microchannel. The influence of Helmholtz-Smoluchowski velocity $\left(Uhs\right)$ on axial pressure gradient is plotted in **Fig. 13** for $Al_2O_3 - CuO$ nanofluid. It is observed that pressure gradient is enhanced markedly with positive values of Helmholtz-Smoluchowski velocity (axial electrical field case) whereas it is suppressed with negative values (reversed electrical field case). **Fig. 14** has been plotted to analyze the impact of Joule heating parameter on pressure gradient for the copper- water based nanofluid case. Increasing Joule electrical dissipation effect (higher values of γ) manifest in a strong escalation in axial pressure gradient at all values of axial coordinate, ξ. This is linked to the qaudratic nature of the electrical field in the Joule heating term, $\gamma = \frac{\sigma d_1 E_\xi^2}{\kappa_f (T_1 - T_0)}$. For vanishing Joule dissipation, $\gamma \to 0$ and minimum pressure gradient magnitudes are computed. **Fig. 15** indicates that for water based-alumina hybrid nanofluid, with increasing slip axial velocity parameter (ξ_1) there is a diminishing in the pressure gradient. Similarly, with increasing thermal slip parameter (ξ_2) for titania-water nanofluid (**Fig. 16**) there is also a reduction induced in the pressure gradient although the effect is less pronounced than for velocity slip in **Fig. 15**. Clearly the imposition of momentum (velocity) and thermal slip (jump) boundary conditions, which can arise in real electro-osmotic systems, is an important feature to include for accurate simulations of these systems [28-31].

3.3 Nanoparticle temperature distribution

The impact of several parameters i.e. $Br, \gamma, Gr, \kappa, \xi_1, \xi_2$ and Uhs on nanoparticle temperature are illustrated in **Figs.17-23** for the fixed value of $\varpi = 0.1$**.** In **Fig.17**, we have examined for alumina-water nanofluid the influence of Brinkman number $\left(Br = Ec\,\mathrm{Pr}\right)$ on the nanoparticle temperature distribution. With greater Brinkman number nanoparticle temperatures are elevated in the left half space of the microchannel whereas they are decreased in the right half space. Viscous dissipation therefore exerts variable effects on temperature field depending on the location in the microchannel. **Fig. 18** has been plotted to observe the effect of Joule heating parameter on nanoparticle temperature distribution for copper-water hybrid nanofluid. An increase in γ is found to elevate nanoparticle temperature magnitudes across the microchannel core although there is a slight depression in values at the walls. **Fig. 19** shows that for alumina-based water nanofluid, the temperature distribution is effectively enhanced in the left half space of the microchannel with increasing thermal Grashof number $\left(Gr\right)$ but decreased in the right microchannel half space. However, these trends are reversed at the walls of the microchannel. **Fig.20** illustrates that for copper-water nanoliquid temperature is unaffected with increasing electro-osmotic parameter (κ) at the peripheral sections of the microchannel (near the walls) whereas it is markedly boosted in the core zone of the microchannel. In the core zone, the minimum temperature is therefore attained for vanishing electroosmosis parameter. **Fig.21** shows that for titania-water nanofluid, an increase in slip axial velocity parameter $\left(\xi_1\right)$ generally elevates the temperature in the left half space of the microchannel whereas it reduces temperature in the right half space, with deviations from these patterns at the walls. **Fig. 22** shows that for alumina-water nanofluid, with increasing thermal slip parameter $\left(\xi_2\right)$, temperatures are decreased at the left wall and entire left half space whereas this behavior is reversed deeper into the right half space of the microchannel where thermal slip boosts temperatures and this is sustained at the right wall. **Fig. 23** depicts the temperature profiles for titania-water nanofluid with various values of Helmholtz-Smoluchowski (electro-osmotic) velocity, *Uhs* with fixed values of other parameters. It is apparent that nanoparticle temperature is a maximum in the core zone and is basically enhanced across the microchannel width with increasing *Uhs* values.

3.4 Validation of the numerical results

The numerical results of present models have been validated with the existing results obtained by the Srinivas and Kothandapani [35] which is a special (non-magnetic) case of the present model for $(M = 0)$ in Fig.24. The axial velocity profile is illustrated for the result of present model and existing model with the following prescribed values of other parameters: $Gr = 0, Uhs = 0, \varpi = 0, \xi_1 = 0, \xi_2 = 0, a = b = 0$. From Fig.24, it is evident that excellent correlation between numerical results of present study and existing results is achieved. Confidence in the present MATLAB solutions is therefore justifiably high.

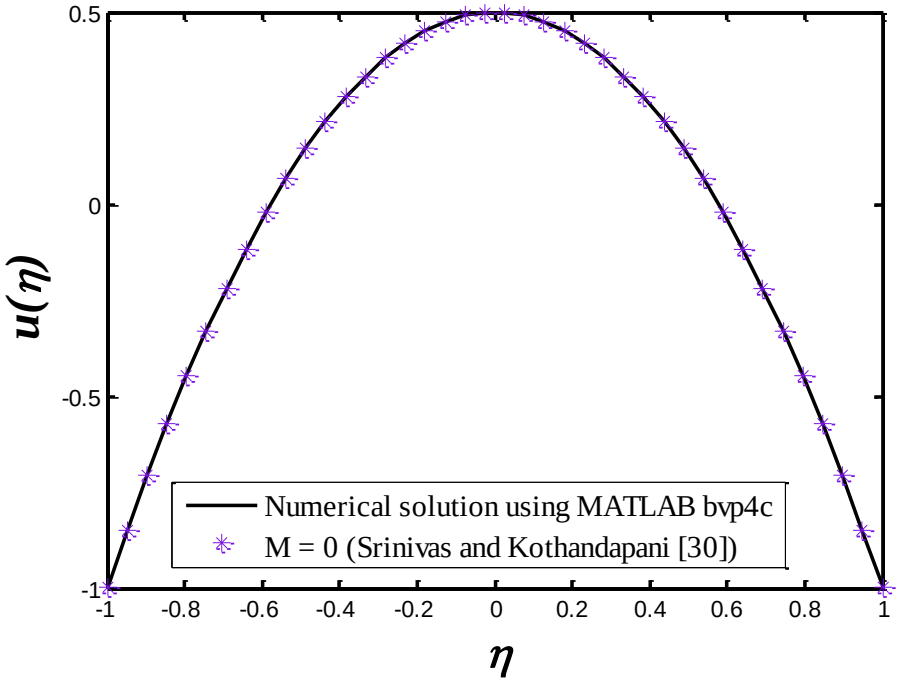

Fig. 24 Validation of Numerical results with existing results of Srinivas and Kothandapani [30] for axial velocity distribution.

4. CONCLUDING REMARKS

In this present study, a theoretical investigation has been conducted for electro-osmotic hybrid nanofluid peristaltic propulsion in a symmetric microchannel with Joule heating. Three different types of water based metallic nanoliquids are utilized and both velocity (momentum) slip and thermal slip boundary conditions are employed. The two-dimensional governing equations have been formulated and then simplified under the lubrication theory and Debye–Hückel linearization.

The numerical solutions for axial velocity, pressure gradient and nanoparticle temperature have been achieved by using the efficient and versatile MATLAB bvp4c command. The computations have shown that:

(i) Pressure gradient is elevated with stronger buoyancy i.e. higher thermal Grashof number and also electroosmosis parameter whereas it is reduced with greater velocity slip and thermal slip parameters.

(ii) Axial flow is strongly accelerated with increasing Joule heating parameter and velocity slip.

(iii) Oscillatory behavior is simulated for axial pressure gradient for all three metallic nanoparticles due to the sinusoidal nature of the pumping.

(iv) With increasing Brinkman number (dissipation parameter), axial pressure gradient is decreased for the alumina (Al_2O_3)-*water nanofluid.*

(v) Temperature is strongly increased with greater Joule heating parameter across the microchannel width for *Cu-water* nanoliquid.

(vi) Temperature is increased for (Al_2O_3)-water nanofluid in the left microchannel half space with increasing thermal Grashof Number whereas it is decreased in the right half space.

(vii) Temperatures are enhanced for titania TiO_2 -water nanoliquid in the left half space with greater velocity slip parameter whereas they are diminished in the right half space.

(viii) The present analysis is relevant to bio-inspired electrokinetic nanofluid micropump designs, microfluidic cooling systems and nanomedicine.

The current study has assumed smooth internal surfaces for the microchannel walls. Future investigations may consider alternative *bio-inspired* designs with ciliated walls, and furthermore, two-way fluid structure interaction (FSI) to better simulate the deformability of the microchannel wall.

Conflict of interest Statement: On behalf of all authors, the corresponding author states that there is no conflict of interest.

REFERENCES

1. Suresh, S., K. P. Venkitaraj, P. Selvakumar, and M. Chandrasekar. Effect of Al2O3–Cu/water hybrid nanofluid in heat transfer. Experimental Thermal and Fluid Science 38 (2012): 54-60.

2. Sarkar, Jahar, Pradyumna Ghosh, and Arjumand Adil. A review on hybrid nanofluids: recent research, development and applications. Renewable and Sustainable Energy Reviews 43 (2015): 164-177.
3. Suresh, S., K. P. Venkitaraj, P. Selvakumar, and M. Chandrasekar. Synthesis of Al2O3–Cu/water hybrid nanofluids using two step method and its thermophysical properties. Colloids and Surfaces A: Physicochemical and Engineering Aspects 388, no. 1-3 (2011): 41-48.
4. Moghadassi, Abdolreza, Ehsan Ghomi, and Fahime Parvizian. A numerical study of water based Al2O3 and Al2O3–Cu hybrid nanofluid effect on forced convective heat transfer. International Journal of Thermal Sciences 92 (2015): 50-57.
5. Minea, Alina Adriana. Hybrid nanofluids based on Al2O3, TiO2 and SiO2: numerical evaluation of different approaches. International Journal of Heat and Mass Transfer 104 (2017): 852-860.
6. Hayat, Tanzila, and S. Nadeem. Heat transfer enhancement with Ag–CuO/water hybrid nanofluid. Results in physics 7 (2017): 2317-2324.
7. Kuharat, S. and O. Anwar Bég, Computational fluid dynamics simulation of a nanofluid-based annular solar collector with different metallic nanoparticles, Heat and Mass Transfer Research Journal, 3 (2019), 1-23.
8. Moldoveanu, Georgiana Madalina, Alina Adriana Minea, Mihai Iacob, Constanta Ibanescu, and Maricel Danu. Experimental study on viscosity of stabilized Al2O3, TiO2 nanofluids and their hybrid. Thermochimica Acta 659 (2018): 203-212.
9. O. Anwar Bég, S. Kuharat, M. Ferdows, M. Das, A. Kadir, M. Shamshuddin, Magnetic nano-polymer flow with magnetic induction and nanoparticle solid volume fraction effects: solar magnetic nano-polymer fabrication simulation, Proc. IMechE-Part N: J Nanoengineering, Nanomaterials and Nano-systems (2019). DOI: 10.1177/ 2397791419838714 (19 pages)
10. Moldoveanu, Georgiana Madalina, Constanta Ibanescu, Maricel Danu, and Alina Adriana Minea. Viscosity estimation of Al2O3, SiO2 nanofluids and their hybrid: an experimental study. Journal of Molecular Liquids 253 (2018): 188-196.
11. O. Anwar Bég, D.E. Sanchez Espinoza, Ayesha Sohail, Tasveer A. Bég and Ali Kadir, Experimental study of improved rheology and lubricity of drilling fluids enhanced with nanoparticles, Applied Nanoscience, 8 (2018) 1069-1090.
12. Huminic, Gabriela, and Angel Huminic. The heat transfer performances and entropy generation analysis of hybrid nanofluids in a flattened tube. International Journal of Heat and Mass Transfer 119 (2018): 813-827.

13. Shehzad, N., A. Zeeshan, and R. Ellahi. Electroosmotic flow of MHD power law Al2O3-PVC nanouid in a horizontal channel: Couette-Poiseuille flow model. Communications in Theoretical Physics 69, no. 6 (2018): 655.
14. Deng, Shuyan. Thermally fully developed electroosmotic flow of power-law nanofluid in a rectangular microchannel. Micromachines 10, no. 6 (2019): 363.
15. Sheikhizad, N., and M. Kalteh. Study of heat transfer of periodic electroosmotic/pressure driven nanofluid flow in a microchannel using the Poisson-Boltzmann Method. Modares Mechanical Engineering 19, no. 3 (2019): 765-776.
16. Zhao, Guangpu, and Yongjun Jian. Thermal transport of combined electroosmotically and pressure driven nanofluid flow in soft nanochannels. Journal of Thermal Analysis and Calorimetry 135, no. 1 (2019): 379-391.
17. Prakash, J., Dharmendra Tripathi, Abhishek Kumar Tiwari, Sadiq M. Sait, and Rahmat Ellahi. Peristaltic pumping of nanofluids through a tapered channel in a porous environment: Applications in blood flow. Symmetry 11, no. 7 (2019): 868.
18. Prakash, J., E. P. Siva, D. Tripathi, and M. Kothandapani. Nanofluids flow driven by peristaltic pumping in occurrence of magnetohydrodynamics and thermal radiation." Materials Science in Semiconductor Processing 100 (2019): 290-300.
19. Noreen, S., M. M. Rashidi, and M. Qasim. Blood flow analysis with considering nanofluid effects in vertical channel. *Applied Nanoscience* 7, no. 5 (2017): 193-199.
20. Riaz, Arshad, M.M Bhatti, R. Ellahi, A. Zeeshan, and Sadiq M Sait. Mathematical analysis on an asymmetrical wavy motion of blood under the influence entropy generation with convective boundary conditions. *Symmetry* 12, no. 1 (2020): 102.
21. Ellahi, R., F. Hussain, F. Ishtiaq, and A. Hussain. Peristaltic transport of Jeffrey fluid in a rectangular duct through a porous medium under the effect of partial slip: An application to upgrade industrial sieves/filters. *Pramana* 93, no. 3 (2019): 34.
22. Alamri, Sultan Z., R. Ellahi, N. Shehzad, and A. Zeeshan. Convective radiative plane Poiseuille flow of nanofluid through porous medium with slip: an application of Stefan blowing. *Journal of Molecular Liquids* 273 (2019): 292-304.
23. Prakash, J., and Dharmendra Tripathi."Electroosmotic flow of Williamson ionic nanoliquids in a tapered microfluidic channel in presence of thermal radiation and peristalsis. Journal of Molecular Liquids 256 (2018): 352-371.
24. Jayavel, Prakash, Ravinder Jhorar, Dharmendra Tripathi, and Martin N. Azese. "Electroosmotic flow of pseudoplastic nanoliquids via peristaltic pumping. Journal of the Brazilian Society of Mechanical Sciences and Engineering 41, no. 2 (2019): 61.

25. Tripathi, Dharmendra, Ashish Sharma, and O. Anwar Bég. Joule heating and buoyancy effects in electro-osmotic peristaltic transport of aqueous nanofluids through a microchannel with complex wave propagation. Advanced Powder Technology 29, no. 3 (2018): 639-653.
26. Prakash, J., Ashish Sharma, and D. Tripathi. Thermal radiation effects on electroosmosis modulated peristaltic transport of ionic nanoliquids in biomicrofluidics channel. Journal of Molecular Liquids 249 (2018): 843-855.
27. Sharma, A., D. Tripathi, R. K. Sharma, and A. K. Tiwari. Analysis of double diffusive convection in electroosmosis regulated peristaltic transport of nanofluids. Physica A: Statistical Mechanics and its Applications 535 (2019): 122148.
28. O.T.Guenat, D.Ghiglione, W.E.Morf, N.F.de Rooij, Partial electroosmotic pumping in complex capillary systems: Part 2: Fabrication and application of a micro total analysis system (μTAS) suited for continuous volumetric nanotitrations, Sensors and Actuators B: Chemical, 72 (2001)273-282.
29. Al-Rjoub, M.F., A.K Roy, S. Ganguli and R.K. Banerjee, Improved flow rate in electro-osmotic micropumps for combinations of substrates and different liquids with and without nanoparticles, ASME J. Electron. Packag. 137(2015): 021001 (11 pages).
30. Jahanshahi, A., Axisa, F., and Vanfleteren, J, Fabrication of a biocompatible flexible electroosmosis micropump Microfluid. Nanofluid., 12 (2012) 771-777.
31. Comandur, K.A. et al., Transport and reaction of nanoliter samples in a microfluidic reactor using electro-osmotic flow, J. Micromechanics and Microengineering, 20 (2010), 035017.
32. F. M. Abbasi, T. Hayat, and F. Alsaadi, Hydromagnetic peristaltic transport of water-based nanofluids with slip effects through an asymmetric channel, International Journal of Modern Physics B, 29 (21) (2015) 1550151.
33. T. Hayat, F. M. Abbasi, B. Ahmad, Numerical study for transport of water based nanofluids through an asymmetric channel with wavy walls, International Journal of Numerical Methods for Heat & Fluid Flow, 25 (8) (2015) 1868 – 1885.
34. T. Hayat, S. Nawaz, F. Alsaadi, M. Rafiq, M. Mustafa, A model for an application to biomedical engineering through nanoparticles, International Journal of Heat and Mass Transfer 101 (2016) 112–120.
35. S. Srinivas and M. Kothandapani, Peristaltic transport in an asymmetric channel with heat transfer – A note, Int. Commun. Heat Mass Transf., 35 (2008) 514-522.